Supplementary Information for "Atomically Phase-Matched Second-Harmonic Generation in a 2D Crystal"

Mervin Zhao[1, 2†], Ziliang Ye[1, 2†], Ryuji Suzuki[3, 4†], Yu Ye[1, 2], Hanyu Zhu[1], Jun Xiao[1], Yuan Wang[1, 2], Yoshihiro Iwasa[3, 4], Xiang Zhang[1, 2, 5]*

[1]*NSF Nanoscale Science and Engineering Center, University of California, Berkeley, CA 94720, USA.*

[2]*Materials Sciences Division, Lawrence Berkeley National Laboratory, Berkeley, CA 94720, USA.*

[3]*Quantum-Phase Electronics Center (QPEC) and Department of Applied Physics, The University of Tokyo, Tokyo 113-8656, Japan.*

[4]*RIKEN Center for Emergent Matter Science (CEMS), Wako 351-0198, Japan.*

[5]*Department of Physics, King Abdulaziz University, Jeddah 21589, Saudi Arabia.*

[†] *These authors contributed equally to this work.*

** Correspondence and requests for materials should be addressed to X. Zhang. (email: xiang@berkeley.edu)*

Contents

S8. References

S1. Photoluminescence mapping

In order to determine crystals containing single-layer MoS_2 in both crystal polytypes, we have used a confocal microscope setup to map the areas with photoluminescence.

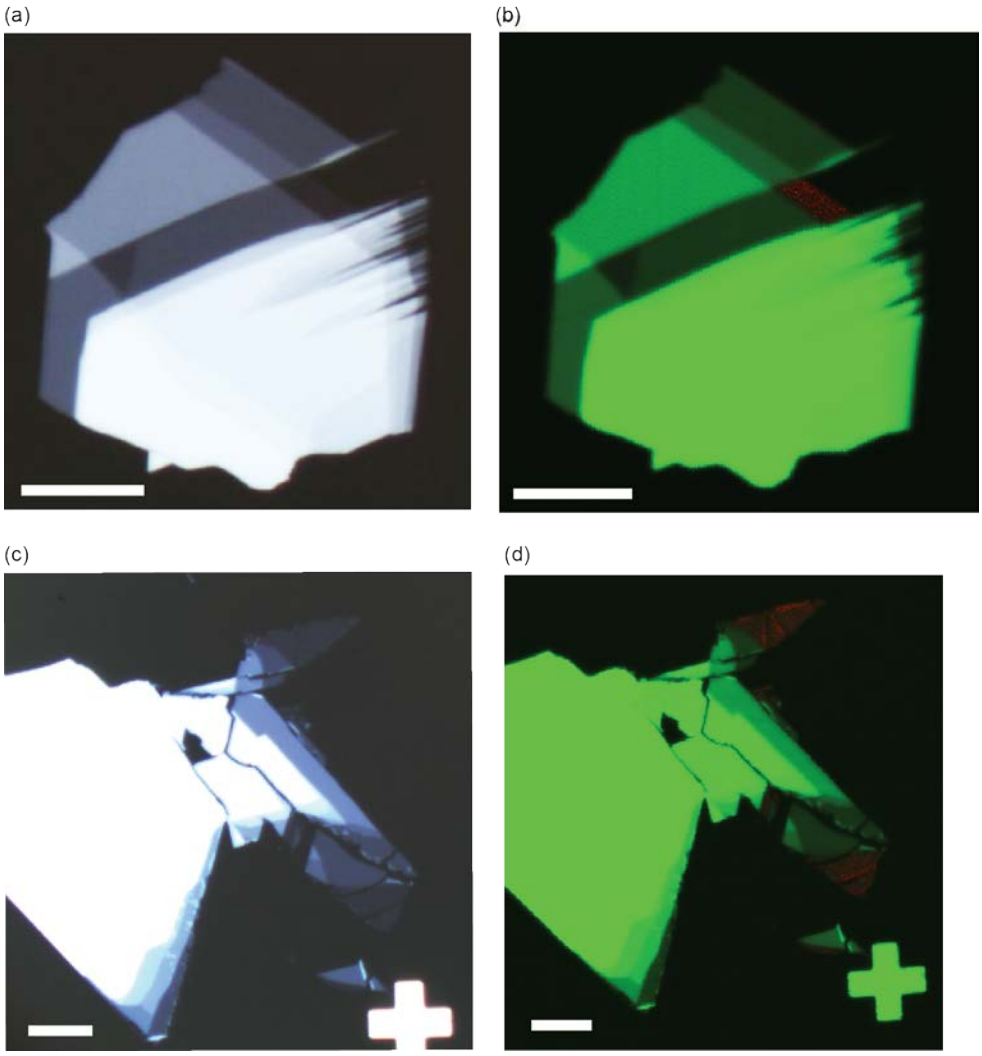

Figure S1. (a) Optical images of the 3R crystal used. (b) Photoluminescence image from the confocal mapping of the 3R crystals. The green channel is the reflection of the excitation laser (488 nm), while the red channel (obtained using a 650 nm long pass filter) is from the single-

layer MoS_2 photoluminescence.[1] (c) Optical images of the 2H crystal used. (d) Photoluminescence image of the 2H crystal. All scale bars correspond to 20 μm.

S2. Raman spectroscopy

We have used the Raman spectra to determine the layer number in both crystal polytypes.[2, 3] We have used the frequency difference between the A_{1g} and E_{2g} peaks.

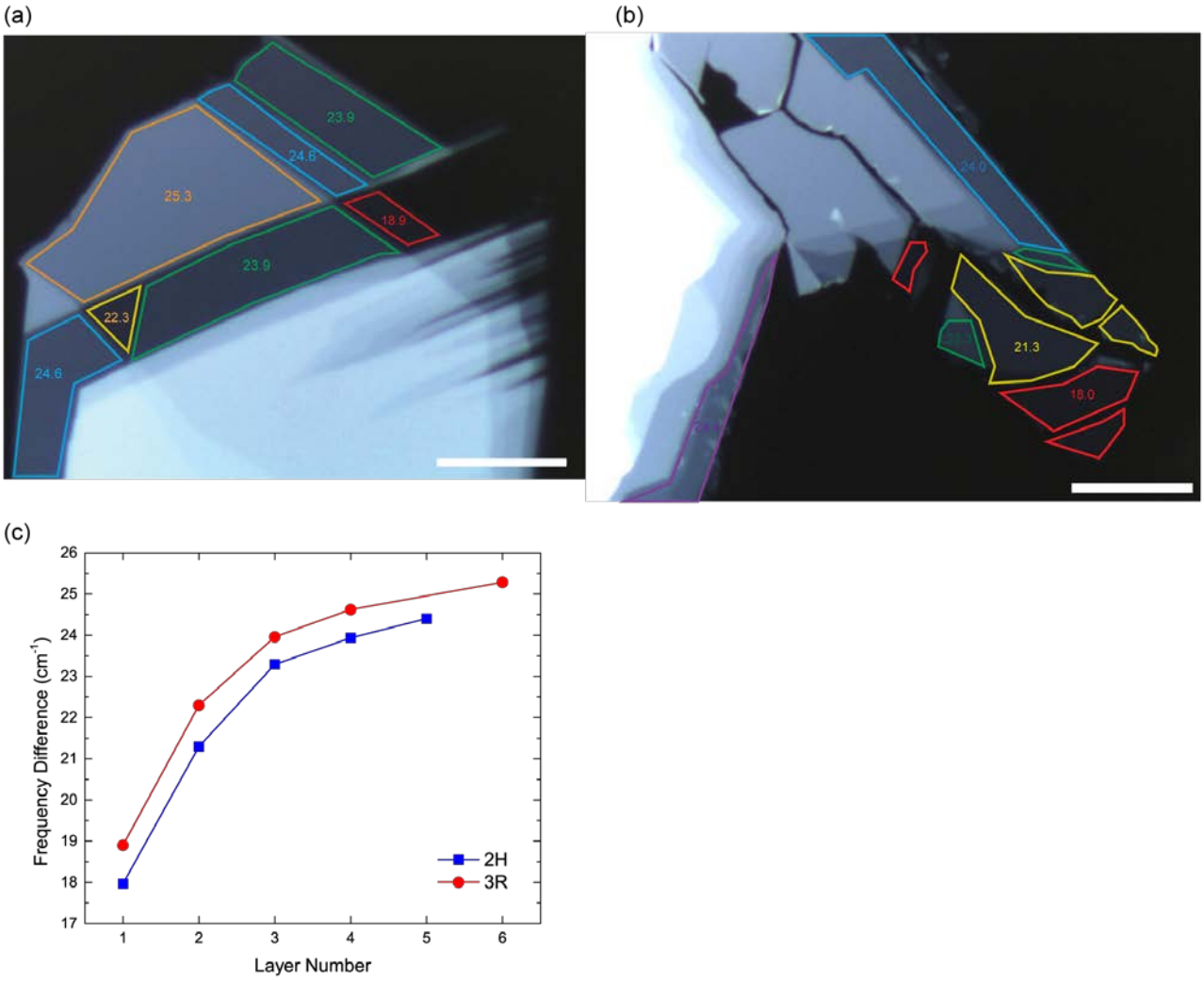

Figure S2. (a) The optical image of the 3R crystals with the experimental Raman frequency differences labeled within the respective crystal areas. (b) Corresponding image of the 2H crystal with frequency differences labeled. (c) Plot of the peak frequency differences along the layer numbers which corresponds well with the reported values.[2, 3] All scale bars correspond to 15 μm.

S3. Atomic force microscopy

We have also confirmed the Raman results using atomic force microscopy (AFM).

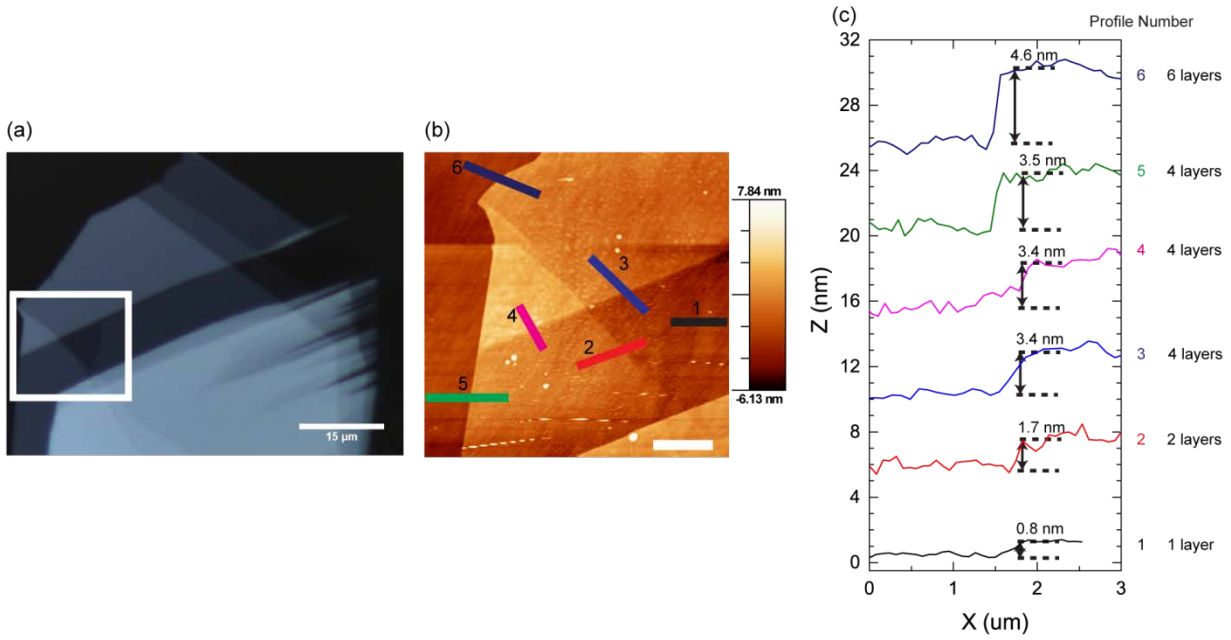

Figure S3. (a) Optical image of the 3R-MoS_2 crystal used. The white boxed area was used for AFM. (b) AFM image corresponding to the boxed area. As the single-layer of the crystal is identical to the well-studied 2H phase we have focused on this smaller area and taken profiles to determine the relative thickness between the layers as well as the absolute thickness taken from the substrate. (c) Profiles corresponding to the six regions marked. These results of step heights confirm the layers assigned using Raman spectroscopy. Each layer was roughly 0.8 nm.

S4. 2H-MoS_2 second harmonic microscopy

We have taken the 2H-MoS_2 SHG here. Stark contrast is shown with the 3R SH microscopy as shown in the main text.

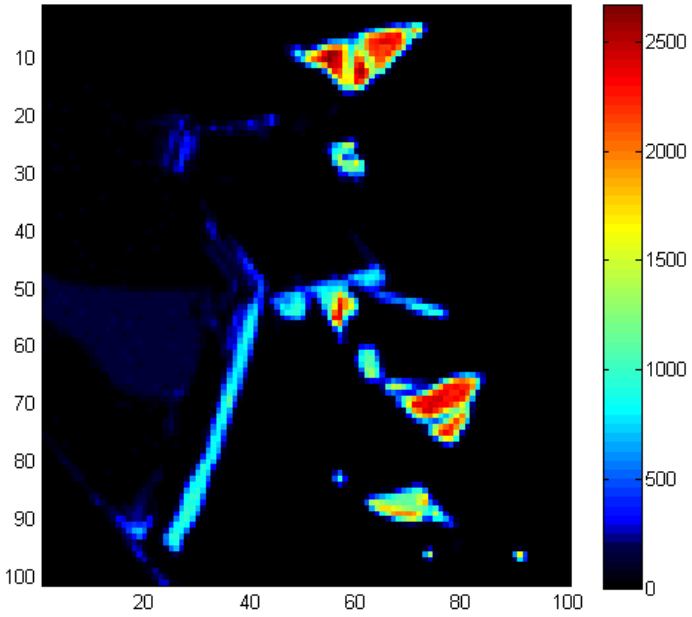

Figure S4. SH mapped image of the 2H-MoS_2 crystal at a SH energy around 2.1 eV. We only see significant intensities from the odd-numbered layers of 1, 3, and 5 (as given in Figure S2.)

S5. 3R-MoS_2 linear absorption

We have taken the linear absorption of the 3R polytype in order to correlate it with the results from SH spectroscopy. In the thicker layers our results agree with previously reported bulk linear absorption.[3]

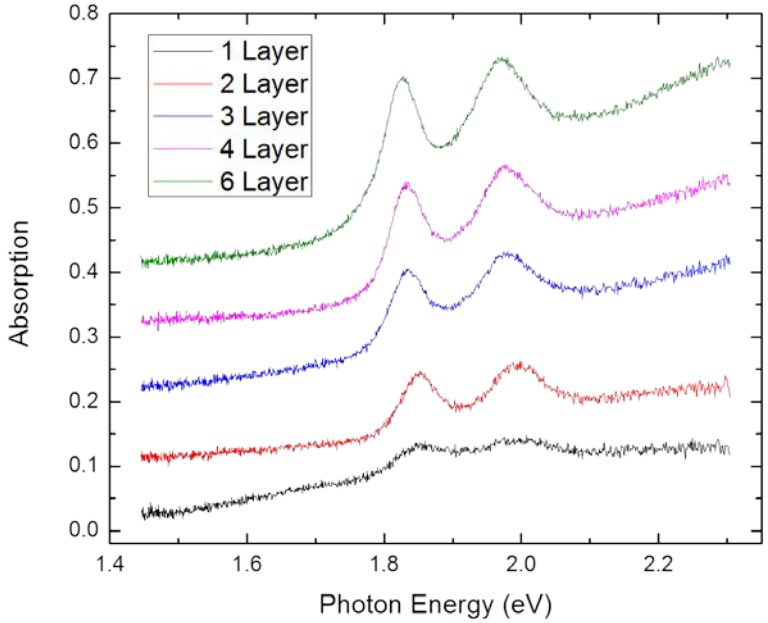

Figure S5. Linear absorption of 3R-MoS_2. We can observe the same features and trend reported in the main text for the SH spectroscopy. The B-exciton feature at around 2.0 eV experiences a larger red shift compared to the A-exciton. However, the peaks are much more clearly observed in the SH spectrum, which gives it advantages in studying these excitonic features.

S6. 3R-MoS_2 SHG phase considerations

Due to any potential refractive index changes which impacts the phase difference of the waves, we have done an analysis of the potential effects of considering the phase difference from the fundamental and second harmonic waves.

In the following, we consider the case where the refractive indices of fundamental and SHG frequencies differ most, namely between infrared fundamental energies (n ~ 4) and second harmonic energies near the exciton peaks (n ~ 6)[4-6]. This will give us the maximum loss due to the phase accumulation. The wave-vector difference Δk, between the fundamental and SH light is:

$$\Delta k = \frac{4\pi}{\lambda_{fund.}}(-n(2\omega) - n(\omega))$$

The additional negative is due to the reflection geometry of the optical setup. For SHG, the field is typically written as:

$$E(2\omega) = -\frac{i\omega d_{\text{eff}}}{n_{2\omega}c}E^2(\omega)\int_0^t e^{i\Delta kz}\,dz$$

While the single layer SHG from MoS_2 is usually presented without any phase factor due to the atomically thin nature (Kumar N, Najmaei S, Cui Q, Ceballos F, Ajayan P, Lou J, *et al.* Second harmonic microscopy of monolayer MoS_2. *Phys Rev B* 2013; **87**: 161403):

$$E(2\omega) = \frac{i\omega}{4n_{2\omega}c}\chi^{(2)}tE^2(\omega)$$

In our analysis where we do not assume any strong interlayer interactions, we treat each layer as optically independent, which allows us to model the individual electric-field from any layer within the 3R-bulk as:

$$E(N, 2\omega) \propto e^{i\Delta k(N-1)t}e^{-\alpha(N-1)t/2}$$

Where $(N-1)$ results due to the indexing of the crystal, i.e. the top-most layer is 1, so the subsequent intensity is normalized to 1, and *t* is the crystal thickness. To account for the reabsorption of the second harmonic light, we introduce an exponential loss, α. This is the attenuation factor at the second harmonic energy extracted from the single-layer linear absorption spectrum, i.e. $\gamma = 1 - I_{abs} = e^{-\alpha t}$, the value of γ in our second harmonic energy range is roughly ~0.9 at the excitonic peaks to ~0.95 at sub-excitonic energies.

We can write the total SH light from *N* layers as:

$$I(N, 2\omega)_{total} \propto \left|\sum_{M=1}^{N} e^{i\Delta k(M-1)t}e^{-\alpha(M-1)t/2}\right|^2$$

Using this general equation as a function of the layer number, refractive indices, fundamental wavelength, and single-layer absorption we calculate some specific cases and compare them to experimental findings. First, we compare the difference introduced using the refractive index changes (Fig S6a).

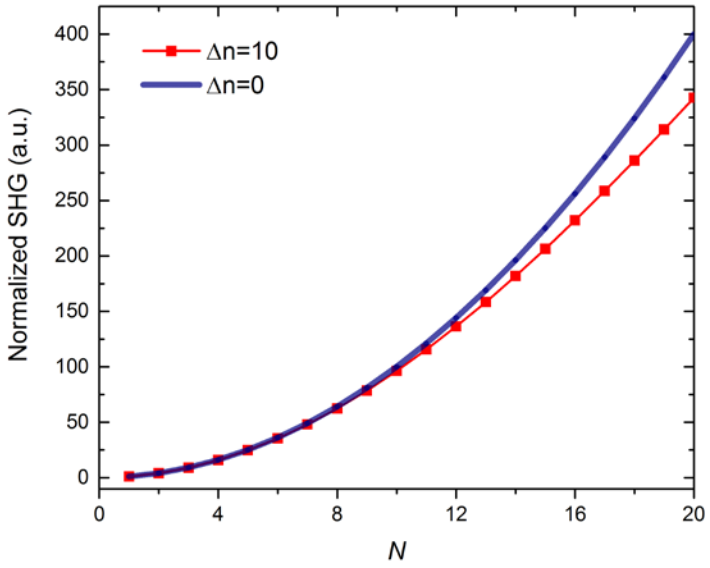

Figure S6a. Plotting the SHG with a refractive index change of 0 and 10. From the plot, we can see that introducing a phase term does not significantly affect the fully ideal SHG (N^2) within ten layers. At around twenty layers there appears to be a deviation of 20% or less.

Introducing the absorption we see that it lies much closer to the experimental data (Fig. S6b). In addition to the plots in the figure above, we add in the loss terms (green and red, respectively) to the cases with no refractive index change and phase accumulation. Here, we use a single layer absorption of 0.05 (i.e. $\gamma = 0.95$), which is an approximate in areas away from the excitonic resonance. At the excitonic resonance the absorption should play an even larger role as there is a large increase, however the modeling of the SHG more complex due to the excitonic peak shifts.

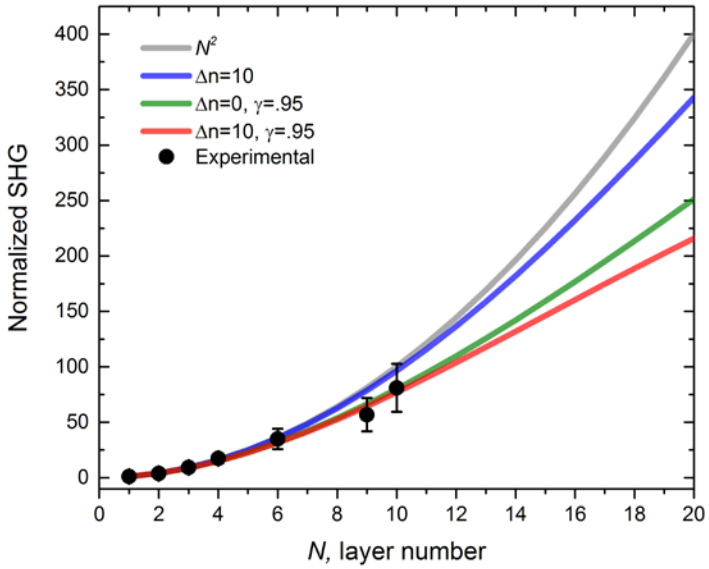

Figure S6b. Plotting the SHG modelled using refractive index changes and absorption changes. Here, we use a single layer absorption of 0.05, which is an approximate in areas away from the excitonic resonance. At the excitonic resonance the absorption should play an even larger role as there is a large increase, however the modeling of the SHG more complex due to the excitonic peak shifts.

From the plot, the experimental data lies very close to the predicted SHG. We see that at six layers, deviations are actually very small, only apparent once it reaches 10 layers or so (which was obtained using the thicker parts of the same crystal). Additionally, we note that the green curve has no phase considerations and only considers the attenuation. Using only the reabsorption matches much closer to the experimental data than the case where there is no absorption. Hence, we conclude that while the refractive index changes play a role, it is actually minimal relative to the attenuation from reabsorption of the SH light within our experimental

limit. Larger deviations as a result of the phase changes may appear after fifteen layers or so (~10 nm).

In conclusion we can summarize the two main causes for the deviation from the predicted N^2 relationship within ten layers. With respect to layer number, the deviations are caused primarily by the reabsorption and slightly by the refractive index changes. Up to six layers, a near N^2 relationship is valid. With respect to the deviations at different SH energies, this is attributed mostly to the excitonic peak shifts, causing varied absorption and phase accumulation in crystals with different layers.

S7. Representative Data

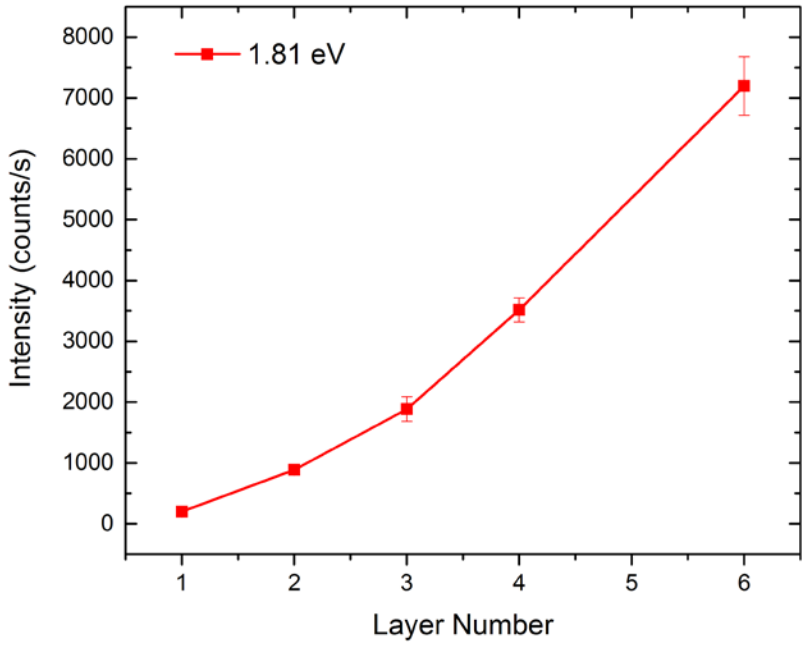

Figure S7. Representative data of the actual error (at 1.81 SH energy to yield for a quadratic dependence) obtained from sampling the crystalline layer's SH signal. The error introduced in the main text's Fig. 3a is actually due to the error propagation, as we see the actual sampling error percentage is much less than that presented in the main text.

S8. References

1. Splendiani A, Sun L, Zhang Y, Li T, Kim J, Chim C-Y, *et al.* Emerging Photoluminescence in Monolayer MoS_2. *Nano Lett.* 2010; **10**: 1271-1275.

2. Lee C, Yan H, Brus LE, Heinz TF, Hone J, Ryu S. Anomalous Lattice Vibrations of Single- and Few-Layer MoS_2. *ACS Nano* 2010; **4**: 2695-2700.

3. Suzuki R, Sakano M, Zhang YJ, Akashi R, Morikawa D, Harasawa A, *et al.* Valley-dependent spin polarization in bulk MoS_2 with broken inversion symmetry. *Nat Nano* 2014; **9**: 611-617.

4. Zhang H, Ma Y, Wan Y, Rong X, Xie Z, Wang W, *et al.* Measuring the Refractive Index of Highly Crystalline Monolayer MoS_2 with High Confidence. *Sci Rep* 2015; **5**: 8440.

5. Chih-Chiang S, Yu-Te H, Lain-Jong L, Hsiang-Lin L. Charge Dynamics and Electronic Structures of Monolayer MoS_2 Films Grown by Chemical Vapor Deposition. *Appl Phys Exp* 2013; **6**: 125801.

6. Li W, Birdwell AG, Amani M, Burke RA, Ling X, Lee Y-H, *et al.* Broadband optical properties of large-area monolayer CVD molybdenum disulfide. *Phys Rev B* 2014; **90**: 195434.